Statistical Analysis of Substorm Events Using The WINDMI Model

Mayowa Kayode-Adeoye, Purbi Adhya, Edmund Spencer

Department of Electrical Engineeering, University of South Alabama (USA), Mobile, United States

Abstract—The SuperMAG magnetic index called the SML index characterizes variations in the Earth's magnetic field due to significant external geomagnetic activities resulting from substorms. This index serves as a crucial parameter for detecting substorm onsets, as utilized by several authors ([1]–[5]). The outputs from the low-order physics-based model WINDMI can also be employed to analyze substorm onsets. In this paper, we evaluate the outputs from the model against the aforementioned techniques to derive criteria for the field-aligned current (FAC) I_1 and its time derivative, both of which are outputs from the model. These criteria hold potential significance in predicting substorm onsets from solar wind data.

Index Terms—SuperMagnetometer (SuperMAG), Substorm Onset, Low-order Physics Model of the Magnetosphere

I. Introduction

The Earth's magnetic field, responsible for shielding the planet from strong geomagnetic activities from the Sun, significantly weakens during storm and substorm events. This occurs as the magnetic field lines reconnect with those from the solar wind, reducing the Earth's magnetic field strength. Through the open field lines, energetic particles from the sun enter Earth's upper atmosphere. Strong storm and substorm events can cause damage to power grids and disrupt satellite communications. Therefore, studying these events is crucial for understanding and forecasting space weather, as well as protecting valuable resources.

Substorms manifest in auroras in higher latitude regions, making the observation of auroras the earliest observational technique employed. The concept of substorms and their different phases were thoroughly observed by several authors for the past few decades ([6]-[8]). In general, substorms involve a sudden release of stored energy in the magnetosphere, with the first phase characterized by a sudden increase in the brightness of the part of a quiet arc near the midnight meridian. This phase is followed by the rapid motion of the arc towards the geomagnetic pole, occurring within about 10-30 minutes. Observational techniques, including auroral images and power spectra, have been employed by various authors to detect substorms, especially their onsets ([1], [2], [9]–[11]). Subsequently, auroral electrojet indices were used to detect substorm onsets, and several numerical observational techniques were employed for studying substorm onsets ([3]–[5]).

This research aims to analyze substorms by employing a low-order plasma physics-based model called the WINDMI model to analyze substorm onsets and compare the model's results with other analytical techniques. Previous research has shown the applicability and success of the model in analyzing

and identifying substorm events ([12]–[14]). Event-by-event analysis was conducted for several substorms using the model ([15]). This study focuses on observing the outputs of the model during a number of substorm events and analyzing the values of the FAC and their slope values. For this purpose, five days were selected, and the substorms that occurred during those days were analyzed. Section II of this paper describes the other techniques compared with the model's outputs. Section III briefly outlines the WINDMI model and its equations. Section IV describes two of the five days studied for this analysis, namely, January 7, 2000, and March 9, 2008 ([16]).

II. SUBSTORM ONSET DETECTION TECHNIQUES

Several comprehensive substorm onset detection techniques have been developed by combining observational data and numerical techniques. Some of these techniques utilize observational data from ground magnetometer stations and, by employing specific rules on that data, detect substorm onsets. The techniques are fully numerical, providing advantages over methods that require the observation of auroral images and potentially manual confirmation of those images to detect substorms from large datasets. Additionally, as magnetometer data are more easily available than auroral images, these methods rarely experience data gaps, making them more suitable for comprehensive substorm analyses. Following are descriptions of three of the techniques:

A. Newell and Gjerloev (2011)

According to the model, onsets are identified at time $= t_0$ when four conditions are satisfied.

$$SML(t_0 + 1) - SML(t_0) < -15nT$$

 $SML(t_0 + 2) - SML(t_0) < -30nT$
 $SML(t_0 + 3) - SML(t_0) < -45nT$

$$\sum_{i=1}^{29} SML(t_0+i) - SML(t_0) < -100nT$$

These conditions dictate that whenever there is a sharp decrease in the SML index, and the SML index stays negative for the next approximately half an hour, there is a substorm.

B. Forsyth et al., (2015)-SOPHIE Model

Primarily, this method divided the durations of strong variations in the SML index into different phases of substorms based on several rules. In their SOPHIE model for detecting substorm onsets, the authors first preprocessed the

SML data with low-pass filtering and three-point Lagrangian interpolation. Subsequently, they calculated the percentile of dSML/dt. The durations corresponding to dSML/dt < 0denoted expansion percentiles (EP), while the durations corresponding to dSML/dt > 0 denoted recovery percentiles. If dSML/dt was negative and |dSML/dt| was greater than a specified EP threshold (EPT), the duration was marked as the expansion phase. Conversely, if dSML/dt was positive and greater than a specified recovery phase (RPT) threshold, the duration was marked as the recovery phase. Whenever successive phases of substorms were observed, the beginning of the expansion phases was marked as possible substorm onsets.

C. Ohtani and Gjerloev (2020)

The substorm onset detection technique obtained by the authors follows several criteria. Their method is a modification of the techniques developed by the technique described in subsection 'A' which detects substorm onsets from identifying sharp decreases in the SML index. Similar to the previous study ([3]), the SML magnitudes must remain strongly negative for about half an hour, for the event to be considered as a substorm. The key aspect of this technique is the onset break that forms at the intersection of the growth phase and the expansion phase which is detected if $\Delta SML/\Delta t^2 \leq$ $-1.5nT/min^2$. This is observed as a knee-like shape in the SML curve.

III. WINDMI MODEL

The WINDMI model ([12], [17]) is a low-order plasmaphysics-based model that takes solar wind data as input and utilizes eight nonlinear ordinary differential equations to determine the energy flow through the magnetosphere-ionosphere system. The model employs the coupled nonlinear equations to track the exchange of electromagnetic, electric, and mechanical energy through eight pairs of energy-conserving terms. These equations encapsulate the intricate dynamics within the magnetosphere-ionosphere system birthed from the compact and flexible six-term analytical representation for the magnetopause field, shielding the Earth's dipole field ([18]).

This model incorporates solar wind data as a dynamo voltage (V_{SW}) , serving as the driving force in the coupled magnetosphere-ionosphere system. Among the many coupling functions that can serve as inputs to the model, we have chosen the half-wave rectified vB_s voltage as input. This voltage is calculated by taking only the southward component of the IMF (Interplanetary Magnetic Field) and multiplying it by the solar wind velocity along the Sun-Earth line. During periods when the IMF was northward, the vB_s value was zero. Specifically, the model focuses on energy flow through the geomagnetic tail and the region 1 (R1) part of the ionosphere, calculating currents, voltages, pressures, and energies in those regions. The model provides a simplified representation of the magnetosphere-ionosphere system under various geomagnetic conditions.

The eight equations of the model are as follows:

$$L\frac{dI}{dt} = V_{\rm sw}(t) - V + M\frac{dI_1}{dt}$$
 (1)

$$C\frac{dV}{dt} = I - I_1 - I_{ps} - \Sigma V \tag{2}$$

$$C\frac{dV}{dt} = I - I_1 - I_{ps} - \Sigma V$$

$$\frac{3}{2}\frac{dp}{dt} = \frac{\Sigma V^2}{\Omega_{cps}} - u_0 p K_{\parallel}^{\frac{1}{2}}\Theta(u) - \frac{pVA_{\text{eff}}}{\Omega_{cps}B_{\text{tr}}L_y} - \frac{3p}{2\tau_E} (3)$$

$$\frac{dK_{\parallel}}{dt} = I_{ps}V - \frac{K_{\parallel}}{\tau_{\parallel}} \tag{4}$$

$$L_I \frac{dI_1}{dt} = V - V_I + M \frac{dI}{dt}$$
 (5)

$$C_I \frac{dV_I}{dt} = I_1 - I_2 - \Sigma_I V_I \tag{6}$$

$$L_2 \frac{dI_2}{dt} = V_I - (R_{\text{prc}} + R_{A2})I_2 \tag{7}$$

$$\frac{dW_{\rm rc}}{dt} = R_{\rm prc}I_2^2 + \frac{pVA_{\rm eff}}{B_{\rm tr}L_y} - \frac{W_{\rm rc}}{\tau_{\rm rc}}$$
 (8)

where $V_{SW}(t)$ is the solar wind dynamo voltage, V and V_I are the voltages of the magnetosphere and ionosphere current loops, respectively. The geotail, region-1, and region-2 currents are denoted as I, I_1 , and I_2 . Similarly, L, C, and Σ represent the inductance, capacitance, and conductance of the geotail, while L_I , C_I , and Σ_I denote the same parameters for the ionosphere. p is the mean plasma sheet pressure over the volume Ω_{cps} , and I_{ps} represents the pressure gradientdriven current. The parallel kinetic energy due to ion mass flowing along the magnetic field lines is denoted as K_{\parallel} , while W_{rc} denotes the ring current energy. A_{eff} is an effective aperture for particle injection into the ring current. M represents the mutual inductance between the two current loops of the magnetosphere and ionosphere. R_{prc} and R_{A2} are the resistances in the partial ring current and the region-2 current I_2 , respectively. τ_E , τ_{\parallel} , and τ_{rc} are the confinement times for the central plasma sheet, parallel kinetic energy, and ring current energy, respectively. The effective width of the magnetosphere is denoted as L_y , and the transition region magnetic field is given by B_{tr} .

For this analysis, we employed the following steps:

- 1) Obtained ACE (Advanced Composition Explorer) data and propagated it by one hour to synchronize with other parameters.
- 2) Calculated the rectified vB_s voltage and added a base voltage of 4kV, which is a nominal viscous voltage required to drive the system.
- 3) Executed the WINDMI model and compared the calculated parameter I_1 with the SML indices.
- 4) Conducted a comprehensive analysis of the WINDMI model results to find the criteria to employ to detect substorm onsets from the outputs of the model.

IV. EVENT BASED ANALYSIS

The statistics of the output from numerical models specified in Section II were compared with the WINDMI model to identify the conditions necessary for applying the WINDMI model to detect substorm onsets. Solar wind data were obtained from

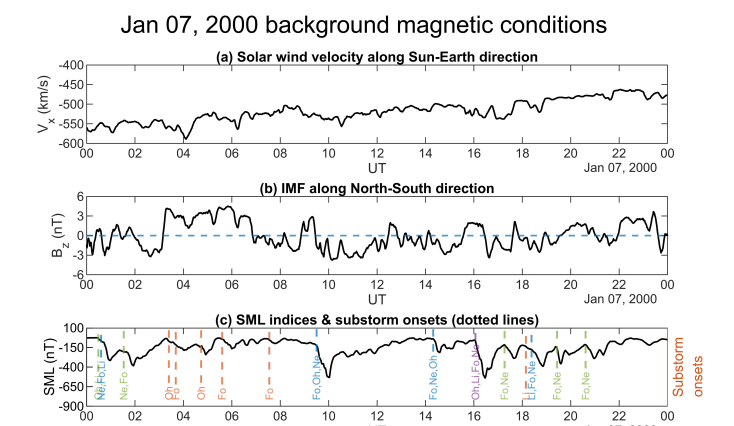


Fig. 1. Background Magnetic Conditions on January 7, 2000. Panel (a) displays the solar wind velocity along the Sun-Earth direction. Panel (b) presents the Interplanetary Magnetic Field (IMF) along the North-South direction. Panel (c) showcases the SuperMAG-based SML indices , and the associated substorm onset times as determined by various techniques.

ACE, and onset times were sourced from SuperMAG. Five days were randomly selected over the course of 17 years to investigate substorm onsets and compare them with the results from the WINDMI model. The studied dates are:

- 1. January 07, 2000
- 2. April 24, 2003
- 3. March 09, 2008
- 4. April 26, 2013
- 5. August 09, 2016

Two of the studied dates, January 07, 2000, and March 09, 2008, are detailed in this paper. The magnetic conditions and substorm events during these two days are initially presented in Figures 1 and 2. Figures 3 and 4 depict the corresponding WINDMI outputs on those dates, with the WINDMI output current I_1 illustrating the FAC analogous to the westward auroral electrojet during substorms.

A. Background Magnetic Conditions

Panel (a) of Figures 1 and 2 presents the representation of the half-wave rectified solar wind input propagated forward by one hour, serving as a fundamental input to the WINDMI model. Panel (b) shows the IMF during the day, with the blue dashed line separating the northward and southward directed fields. Panel (c) provides an illustration of the SuperMAG-based SML indices.

In Panel (c), the colored vertical dotted lines demarcates substorm onsets detected at those specific times through various techniques. The colors assigned to these onsets signify the number of techniques that coincidentally detected each substorm event. Specifically, shades of purple, blue, green, and red correspond to four, three, two, and one method(s) detecting the onsets, respectively. Moreover, in Panel (c), the labels associated with the substorm onsets are abbreviations representing the authors who developed the techniques employed for detection. This comprehensive visualization enables a detailed examination of substorm occurrences and the convergence or



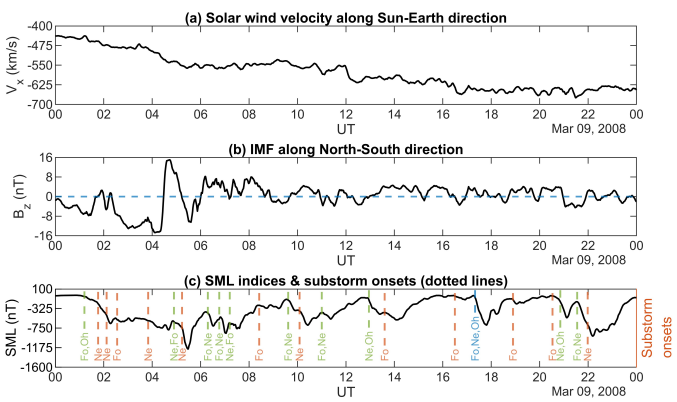


Fig. 2. Background Magnetic Conditions on March 9, 2008. Panel (a) displays the solar wind velocity along the Sun-Earth direction. Panel (b) presents the IMF along the North-South direction. Panel (c) showcases the SuperMAGbased SML indices, and the associated substorm onset times as determined by various techniques.

divergence of detection methods, providing a scientific basis for understanding the dynamics and characteristics associated with geomagnetic substorm events.

On January 07, 2000, high solar wind velocities were observed as seen in Panel (a) of the figure. Simultaneously, the IMF was substantially southwards frequently which created ideal conditions for substorms to occur (Panel (b)). Panel (c) shows that on that day, many substorm onsets were detected by Newell, Forsyth and Ohtani, and some by Liou.

Figure 2 presents the same parameters observed in Figure 1 during March 09, 2008. Throughout the day, the IMF exhibited strong southward components, especially during the first half of the day. Consequently, this led to notable substorm events and depletions in the SML indices during those times. Many of these depletions were identified as substorm onsets by Newell, Forsyth, and Ohtani.

B. WINDMI outputs

In this study, our objective was to establish suitable criteria for detecting substorms from the outputs of the WINDMI model. Since our focus was on observing substorm onsets, we primarily concentrated on the state variable I_1 , representing the R1 FAC. During substorm occurrences, heightened particle deposition in the polar regions leads to a substantial increase in the FAC, closing through the ionosphere. This increase manifests as a change in the Earth's surface magnetic field, i.e., the SML index. Consequently, the FAC reasonably corresponds to the SML index. Similar to other techniques, our approach involved utilizing changes in the SML index and hence the FAC to identify substorms. By adopting rules that detect sharp changes and prolonged negativity in the SML values during substorms, we explored the possibility of employing specific criteria based solely on the FAC index I_1 for substorm onset detection in the WINDMI model outputs. Our primary research goal was to establish this relationship and compare the results with actual substorm onsets, assessing

Fig. 3. WINDMI Outputs for January 7, 2000, with L=100~H and C=50000~F. Panel (a) shows the half-wave rectified solar wind input. Panels (b) and (c) depict FAC I1 and its slope. Panel (d) presents SML indices. Colored vertical dotted lines indicate substorm onsets detected by various techniques, with colors representing the number of techniques coincidentally detecting the specific substorm. Panel (d) labels are abbreviations of the authors who invented the techniques: Forsyth [4], Frey [1], Liou [2], Newell [3], and Ohtani [5].

how well WINDMI outputs align with substorm onset data identified by the techniques mentioned in Section II.

In Figures 3 and 4, we use nominal values of L and C, i.e., L = 100 H and C = 50000 F ([12]) to show the outputs obtained during the two dates, January 07, 2000 and March 09, 2008. The Panel (a) in the figures show the half-wave rectified input vB_s that acts as the input to the model for the two days. Panels (b) and (c) show the output current I_1 and its derivative with respect to time. The last panel shows the SML indices during the day for comparison of the WINDMI output with the SML index and the detected substorm onsets. The dotted lines in Panels (b), (c) and (d) are the substorm onsets detected by the other techniques. Panels (d) in Figures 1 and 2 are identical to panels (c) in Figures 3 and 4.

Panel (b) in Figure 3 displays multiple peaks in the output I_1 , indicating enhancements in FACs during the day. A drawback of the model is the presence of negative current values. The current values exhibit several instances of rise throughout the day, with the ascent vaguely corresponding to the solar wind input as the model operates using this input. The magnitude of the current often reaches almost 800 kA during substorms. In Panel (c), the slope of the current, represented by the parameter dI_1/dt , exhibits significantly high magnitudes several times throughout the day, corresponding to the observation of high-magnitude substorms. The magnitudes of the slopes often reach up to 10 kA/min during these substorms.

To further analyze the magnitudes of the output FAC I_1 and its time derivative dI_1/dt during substorms, maximum values of these parameters were extracted within 15-minute windows on either side of the detected substorm onsets by other methods

Mar 09, 2008 WINDMI outputs with nominal L and C

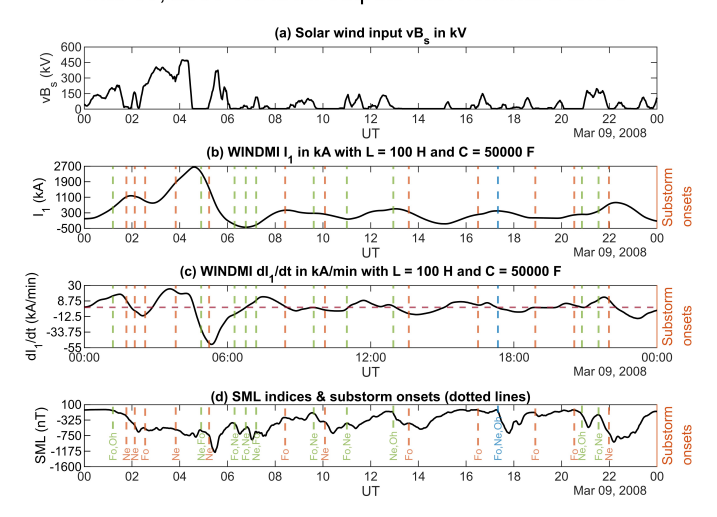


Fig. 4. WINDMI Outputs for March 9, 2008, with L=100~H and C=50000~F. Panel (a) shows the half-wave rectified solar wind input. Panels (b) and (c) depict FAC I1 and its slope. Panel (d) presents SML indices. Colored vertical dotted lines indicate substorm onsets detected by various techniques, with colors representing the number of techniques coincidentally detecting the specific substorm. Panel (d) labels are abbreviations of the authors who invented the techniques: Forsyth [4], Frey [1], Liou [2], Newell [3], and Ohtani [5].

throughout all substorm events on the five selected days. These values are presented as heatmaps in Figures 5 and 6. The heatmaps illustrate the correspondence between the current I_1 and the slope dI_1/dt , as well as the correspondence between the slope dI_1/dt and the slope of the SML index dSML/dt. The first heatmap showcases the magnitudes of the output parameters during substorms, while the second heatmap aims to reveal the correlation between WINDMI output and the SML values, as well as the detected substorm onsets identified by other methods.

C. Statistical Analyses

To establish criteria for analyzing solar wind data through the WINDMI model, our focus was on selecting thresholds for the FAC output I_1 from the model and its derivative. Specifically, we examined the maximum values within 15-minute windows on either side of the substorm onsets detected by various techniques. The objective was to observe whether the magnitudes of these values cluster in the heatmaps, enabling us to set thresholds accordingly while predicting substorms in the future. This approach aimed to identify patterns and concentrations of values that can guide the determination of conditions for solar wind data analysis using the WINDMI model.

Figure 5 shows the heatmap for maximum FAC I_1 and dI_1/dt surrounding substorm onsets. The heatmap analysis depicts the distribution of substorm onsets concerning the maximum FAC I_1 and its time derivative dI_1/dt . The I_1 values are categorized into 10 bins ranging from 0 to 3000 kA, with labels representing the first value of each bin, and each bin covering a range of 300 kA. For dI_1/dt , the number

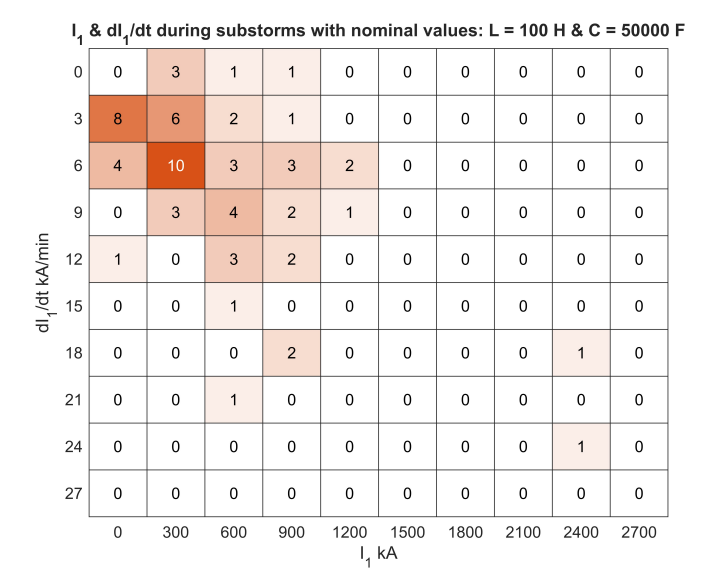


Fig. 5. Heatmap analysis for the maximum FAC I_1 and its time derivative dI_1/dt surrounding substorm onsets. I_1 is divided into 10 bins from 0 to 3000 kA, each spanning 300 kA. For dI_1/dt , the number of bins is the same, covering a range of 0 to 30 kA/min, with each bin spanning 3 kA/min. The heatmaps illustrate the counts of substorm onsets for the corresponding bins. I_1 and dI_1/dt are calculated by taking the maximum values within a 30-minute time window before and after the detected substorm onsets. If substorms occur within this boundary, they are considered as the boundaries for the time period.

of bins is consistent, covering a total range of 0 to 30 kA/min, with each bin spanning 3 kA/min. The heatmaps illustrate the counts of substorm onsets corresponding to the respective bins. The calculation of I_1 and dI_1/dt involves determining their maximum values within a time window spanning 30 minutes before and after the detected substorm onsets. Substorms occurring within this 30-minute boundary on either side are considered as the limits for the time period.

The figure illustrates that the majority of the magnitudes of I_1 cluster within the 300-600 kA and 600-900 kA bins, suggesting that during substorms, I_1 exhibits an enhancement reaching a maximum in these ranges. A similar clustering pattern is observed along the dI_1/dt axis, indicating that values cluster at the 3-6 kA/min and 6-9 kA/min bins. Notably, the 300-600 kA I_1 and 6-9 kA/min dI_1/dt bin exhibits the highest number of substorm events, totaling 10. Some exceptionally high current values, ranging within 2400-2700 kA, were observed during the five studied days. Slope values for currents reach a maximum of 21-24 kA/min among these days.

Figure 6 presents the distribution of substorm onsets concerning the maximum FAC I_1 and its time derivative dI_1/dt . The I_1 values are categorized into 10 bins ranging from 0 to 3000 kA, with labels representing the first value of each bin and each bin covering a range of 300 kA. For dI_1/dt , the number of bins is consistent, covering a total range of 0 to 30 kA/min, with each bin spanning 3 kA/min. The heatmaps illustrate the counts of substorm onsets corresponding to the respective bins. The calculation of I_1 and dI_1/dt involves

dSML/dt & dl /dt during substorms with nominal values: L = 100 H & C = 50000 F

		1									
dl ₁ /dt kA/min	0	0	0	0	0	1	0	0	2	0	2
	3	0	0	0	0	0	0	2	0	8	8
	6	0	0	0	0	0	0	0	6	13	3
	9	0	0	0	0	0	1	0	2	5	3
	12	0	1	0	0	0	0	0	0	5	0
	15	0	0	0	0	0	0	0	0	0	1
	18	0	0	0	0	0	0	0	0	3	0
	21	0	0	0	0	0	0	0	0	0	1
	24	0	0	0	0	0	0	0	0	0	1
	27	0	0	0	0	0	0	0	0	0	0
		-300 -270 -240 -210 -180 -150 -120 -90 -60 -30 dSML/dt nT/min									

Fig. 6. Heatmap analysis for the maximum rates of change of FAC (dI_1/dt) and SML index (dSML/dt) surrounding substorm onsets. dI_1/dt is divided into 10 bins from 0 to 30 kA/min, each spanning 3 kA/min. For dSML/dt, the number of bins is the same, covering a range of -300 to 0 nT/min, with each bin spanning 30 nT/min. The heatmaps illustrate the counts of substorm onsets for the corresponding bins. For dSML/dt, the maximum values are determined from the onset of the substorm and extend to 30 minutes after the onset time.

determining their maximum values within a time window spanning 30 minutes before and after the detected substorm onsets. Substorms occurring within this 30-minute boundary on either side are considered as the limits for the time period.

The heatmap reveals a strong correlation between the time derivative of the WINDMI output I_1 , dI_1/dt , and the time derivative of the SML index dSML/dt. The values cluster predominantly in the 6-9 kA/min and -60 to -30 nT/min bin. This clustering indicates that dSML/dt values tend to concentrate around -60 to -30 nT/min, as derived from the conditions imposed by other numerical techniques. These techniques utilize a threshold for the slope of the SML index to detect substorm onsets.

V. DISCUSSSION

The WINDMI model's outputs, despite being a low-order plasma physics model, have demonstrated notable success in showing a correlation with the SML index during substorm onsets when provided with solar wind data. While the study focused on only five days, these days experienced a heightened number of substorm events due to increased geomagnetic activities. Consequently, many other techniques successfully identified substorm onsets during these days, often detecting the same events. Utilizing data from the ACE satellite, which provides solar wind data before it reaches the nose of the magnetosphere, the WINDMI model aims to predict substorm onsets approximately an hour ahead of time—roughly the time taken by the solar wind to reach the magnetosphere's nose.

While not strictly linear, the clustering tendencies in the data indicate a strong correlation between the I_1 values, its time

derivative dI_1/dt , and their correspondence to the variation in the SML indices.

VI. CONCLUSIONS

In conclusion, our study focused on establishing criteria for analyzing solar wind data through the WINDMI model by selecting thresholds for the FAC output I_1 and its derivative. The analysis involved examining maximum values within 15-minute windows around substorm onsets detected by various techniques, aiming to identify clustering patterns that could guide the determination of analysis conditions.

The heatmaps provided insights into the distribution of substorm onsets based on the maximum FAC I_1 and its time derivative dI_1/dt . The clustering tendencies revealed that during substorms, I_1 tends to exhibit enhancements in the 300-600 kA and 600-900 kA bins, with a similar clustering pattern observed in dI_1/dt at 3-6 kA/min and 6-9 kA/min bins. The 300-600 kA I_1 and 6-9 kA/min dI_1/dt bin showed the highest number of substorm events. Additionally, exceptionally high current values were observed, reaching up to 2400-2700 kA, and slope values for currents reached a maximum of 21-24 kA/min. These high current values quantify the intensity of geomagnetic disturbances in the magnetosphere. The large current values observed in Panel (b) of Figure 4 were due to very high vB_s values (greater than 400 kV).

Furthermore, the strong correlation between the time derivatives of WINDMI output I_1 , dI_1/dt , and SML index dSML/dt was evident in the heatmaps. The clustering at 6-9 kA/min and -60 to -30 bin in the dI_1/dt -dSML/dt heatmap indicated that dSML/dt values tended to concentrate around -60 to -30 nT/min. These values of I_1 and dI_1/dt could be used to predict substorm onsets. The conditions imposed by other numerical techniques, which use a threshold for the slope of the SML index to detect substorm onsets, along with the high correlation of I_1 with the SML, showcase the potential of the WINDMI model in predicting substorm onsets.

REFERENCES

- [1] H. Frey, S. Mende, V. Angelopoulos, and E. Donovan, "Substorm onset observations by image-fuv," *Journal of Geophysical Research: Space Physics*, vol. 109, no. A10, 2004.
- [2] K. Liou, "Polar ultraviolet imager observation of auroral breakup," *Journal of Geophysical Research: Space Physics*, vol. 115, no. A12, 2010.
- [3] P. Newell and J. Gjerloev, "Substorm and magnetosphere characteristic scales inferred from the supermag auroral electrojet indices," *Journal of Geophysical Re*search: Space Physics, vol. 116, no. A12, 2011.
- [4] C. Forsyth, I. Rae, J. Coxon, *et al.*, "A new technique for determining substorm onsets and phases from indices of the electrojet (sophie)," *Journal of Geophysical Research: Space Physics*, vol. 120, no. 12, pp. 10–592, 2015.

- [5] S. Ohtani and J. W. Gjerloev, "Is the substorm current wedge an ensemble of wedgelets?: Revisit to midlatitude positive bays," *Journal of Geophysical Research: Space Physics*, vol. 125, no. 9, e2020JA027902, 2020.
- [6] S.-I. Akasofu, "The development of the auroral substorm," *Planetary and Space Science*, vol. 12, no. 4, pp. 273–282, 1964.
- [7] G. Rostoker, S.-I. Akasofu, J. Foster, *et al.*, "Magnetospheric substorms—definition and signatures," *Journal of Geophysical Research: Space Physics*, vol. 85, no. A4, pp. 1663–1668, 1980.
- [8] R. L. McPherron, "Magnetospheric substorms," *Reviews of Geophysics*, vol. 17, no. 4, pp. 657–681, 1979.
- [9] H. Frey and S. Mende, "Substorm onsets as observed by image-fuv," in *Int. Conf. Substorms*, vol. 8, 2006, pp. 71–75.
- [10] Y. Nishimura, L. Lyons, S. Zou, et al., "Preonset time sequence of auroral substorms: Coordinated observations by all-sky imagers, satellites, and radars," *Journal* of Geophysical Research: Space Physics, vol. 115, no. A5, 2010.
- [11] L. R. Lyons, Y. Zou, Y. Nishimura, B. Gallardo-Lacourt, V. Angelopulos, and E. F. Donovan, "Stormtime substorm onsets: Occurrence and flow channel triggering," *Earth, Planets and Space*, vol. 70, pp. 1–10, 2018.
- [12] E. Spencer, W. Horton, and I. Doxas, "The dynamics of storms and substorms with the windmi model," *Advances in Space Research*, vol. 38, no. 8, pp. 1657–1668, 2006.
- [13] E. Spencer, S. K. Vadepu, P. Srinivas, S. Patra, and W. Horton, "The dynamics of geomagnetic substorms with the windmi model," *Earth, Planets and Space*, vol. 70, no. 1, pp. 1–9, 2018.
- [14] P. G. Srinivas, E. A. Spencer, S. K. Vadepu, and W. Horton Jr, "Substorm electric and magnetic fields in the earth's magnetotail: Observations compared to the windmi model," in AGU Fall Meeting Abstracts, vol. 2017, 2017, SM31A–2616.
- [15] E. Spencer, P. Srinivas, and S. Vadepu, "Global energy dynamics during substorms on 9 march 2008 and 26 february 2008 using satellite observations and the windmi model," *Journal of Geophysical Research: Space Physics*, vol. 124, no. 3, pp. 1698–1710, 2019.
- [16] M. M. Kayode-Adeoye, "Initiation criteria for the onset of geomagnetic substorms based on auroral observations and electrojet current signatures," *Theses and Disserta*tions, Graduate School, University of South Alabama, 2023.
- [17] W. Horton, M. Pekker, and I. Doxas, "Magnetic energy storage and the nightside magnetosphere-ionosphere coupling," *Geophysical research letters*, vol. 25, no. 21, pp. 4083–4086, 1998.
- [18] N. A. Tsyganenko, "Effects of the solar wind conditions in the global magnetospheric configurations as deduced from data-based field models," in *International confer*ence on substorms, vol. 389, 1996, p. 181.